TRANSMISSION ELECTRON DIFFRACTION IN TE MODIFIED TIO_2

by

Ian James

A senior thesis submitted to the faculty of

Brigham Young University

in partial fulfillment of the requirements for the degree of

Bachelor of Science

Department of Physics and Astronomy

Brigham Young University

April 2008

BRIGHAM YOUNG UNIVERSITY

DEPARTMENT APPROVAL

of a senior thesis submitted by

Ian James

This thesis has been reviewed by the research advisor, research coordinator, and department chair and has been found to be satisfactory.

Date	Bret Hess, Advisor
Date	Eric Hintz, Research Coordinator
Date	Ross L. Spencer, Chair

ABSTRACT

TRANSMISSION ELECTRON DIFFRACTION IN TE MODIFIED TIO_2

Ian James

Department of Physics and Astronomy

Bachelor of Science

Photodarkening tellurium modified TiO_2 nanoparticles exhibit TiO_2 phase change from anatase and brookite when annealed below 700°C, to rutile when annealed at or above 700°C. An increase in size accompanies the phase change and causes smaller nanocrystals to become visible which cling to the surface of the larger rutile crystals. The smaller crystals are composed of TeO_2, as identified by diffraction, and disappear when exposed to the electron beam (observed by TEM) for brief amounts of time. Anatase, brookite and rutile forms of TiO_2 are compared by diffraction. A possible cause of photodarkening in samples annealed at 600°C is the occurrence of surface interactions between Te and anatase or brookite. These surface interactions may be energetically allowed by annealing samples at temperatures near the TiO_2 phase change temperature.

ACKNOWLEDGMENTS

I would like to thank Jeffery Farrer for his endless help in keeping the Technai TF20 up and running, and for answering any questions about TEM that I posed to him. I would like to thank Dr. Hess as well for his patience and good attitude while I worked through things. Also, I would like to acknowledge Steven Philips and all of the great work he did both in researching and presenting about Te modified TiO_2 photodarkening.

Contents

List of Figures

Chapter 1

Introduction

1.1 Hydrogen fuel and semiconductors

Hydrogen fuel technology is a promising field of research that has attracted much attention in the end of the 20th century. Hydrogen fuel has many properties that make it a strong candidate for succeeding fossil fuels as a global primary fuel source. It is environmentally clean, producing pure water when burned. It is also an effective way of storing energy, and can be readily converted to heat or electricity. Finally, as a fuel source, it is inexhaustible. The challenge lies in finding a cheap and effective way of producing hydrogen. Presently, the use of semiconductors in photoelectrolysis is under heavy research.

Photo-electrolysis hinges on the science of semiconductor liquid interfaces, which began with A. E. Becquerel, a French physicist. In 1839, Becquerel noticed that a silver chloride electrode in an electrochemical cell had a photovoltaic effect when illuminated [4]. This became known as the Becquerel Effect.

Little research was done in the field, however, until more was known about solid state physics. Between 1950 and 1970 semiconductor research grew impressively with

investigations into many semiconductors including titanium dioxide. In 1970, TiO_2 was successfully used as a photocatalyst to convert water into hydrogen and oxygen by illumination. This sparked interest in powering electrolysis with sunlight, and led to the investigation of photo-electrolysis.

Photo-electrolysis works around the semiconductor-liquid interface. When photons impinge on the semiconductor, electrons in the valence band are excited to the conduction band and create an electron hole base pair. In the presence of water, the hole accepts electrons from the oxygen in water, while the free electron in the conduction band reduces the hydrogen in water, thus disrupting the molecule. A more detailed description of the process is given by Nozik and Memming [4] [3].

Doping TiO_2 with carbon narrows the band gap, thereby increasing the spectrum of radiation that would create an electron hole base pair. Other elements are being investigated for use as doping substances to create a semiconductor that absorbs visible light. [1]. Our research group noticed that Te modified TiO_2 exhibited photodarkening from an eggshell white to an orange/brown color when exposed to visible light. Steven Philips, a member of our research group, is studying the mechanism of the photodarkening in his thesis. In this thesis I have studied the structure of the Te modified TiO_2 using transmission electron microscopy.

1.2 Principles of TEM

1.2.1 TEM

Electron microscopy allows us to study objects that are smaller than the wavelengths of visible light. In the study of atomic crystal structure, subatomic resolution becomes necessary, and electron microscopes become essential. In a transmission electron microscope, electrons are typically accelerated across a 200 KV potential and emitted

from a field emission gun (FEG) at the top of the scope. This gives the electrons a certain velocity as shown by

$$eV = 1/2 * m * v^2 \tag{1.1}$$

Where e is the charge of an electron and V is the accelerating potential. This velocity is directly related to the wavelength of the electrons by the de Broglie equation:

$$\lambda = h/(m * v) \tag{1.2}$$

Where h is Plank's constant. By reconciling these two equations, we see that

$$\lambda = h/\sqrt{2 * meV} \tag{1.3}$$

Therefore the electrons being emitted by the FEG gun of the Technai TF20 microscope (which are accelerated across a 200KV potential) have a wavelength of about 2.74 pm. This is about one tenth the width of a helium atom, meaning that the electrons are capable of resolving most atoms. Unfortunately the microscope's optics are not perfect, and lens abberations and astigmatism prevent it from reaching such high resolutions. However, the microscope can can still easily resolve nanocrystals that are several nanometers across [5].

After being emitted from the gun, the electrons pass through a series of condenser lenses and apertures that focus them into a moderately uniform beam, which illuminates the sample. After passing through the sample, the electrons are focused by the objective lens. They then pass through two apertures, the diffraction lens, and a series of projector lenses which focus the electrons to form an image on the viewing screen. Because the lenses are magnetic fields, their focal lengths can be changed by changing the amount of current in the coils generating them.

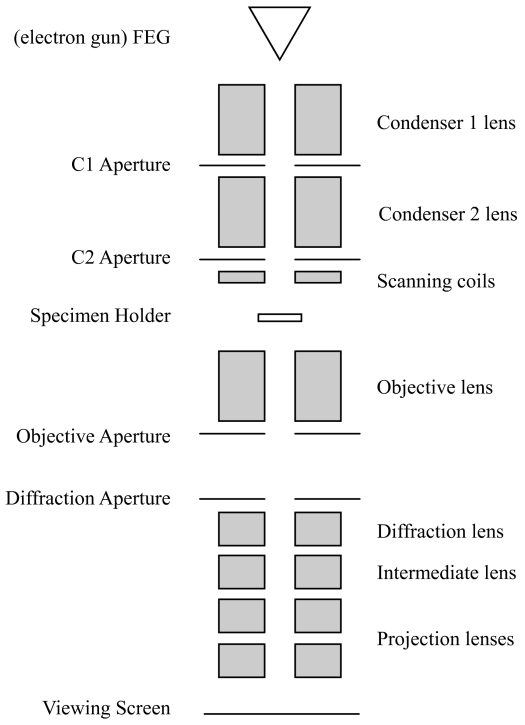

Figure 1.1 The layout of a Transmission Electron Microscope

1.2.2 Diffraction Microscopy

Each spot in a diffraction pattern contains information about the entire grating that created it, making a diffraction pattern a very useful tool for crystallographers. The direction and distance from the center of the screen at which each diffraction spot appears is determined by Bragg's Law as shown in Figure 1.2. The electrons can be considered as waves that reflect off of the atoms in the crystal and then interfere as they propagate to the viewing screen. In order to get constructive interference and produce a diffraction spot,

$$2dsin(\theta) = n\lambda \tag{1.4}$$

Bragg's Law - see Figure 1.2

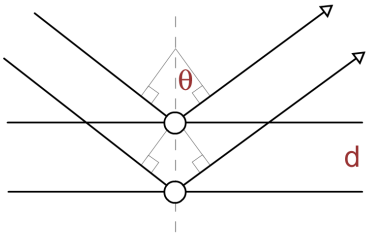

Figure 1.2 Bragg's Law

If we let n = 1, and consider the small angle approximation that holds for the case of electron diffraction, Bragg's Law simplifies to

$$2\theta = \lambda/d \tag{1.5}$$

Next, we consider the angle that the diffracted beam makes with the undeviated beam, and see that it is in fact, 2θ. This angle, in addition with the height of the specimen above the viewing screen will determine the distance of the diffraction spot from the center of the screen by the following relation:

$$tan(2\theta) = R/L \tag{1.6}$$

Where L is a constant called the camera constant that takes into account the multiple focusing effects of the post-specimen lens system, and R is the distance from the center of the screen to the diffraction spot.

Again employing the small angle approximation and reconciling Equation 1.6 with Equation 1.5 above, we see that

$$R/L = \lambda/d \tag{1.7}$$

While our model so far has only considered a few atomic planes in two dimensions, actual nanocrystals constitute many atomic planes in 3 dimensions. When the electron beam looks down an axis that is parallel to several planes so that the atoms in

the crystal appear as columns, the crystal is called "in zone." This creates a lattice of spots on the viewing screen that has a reciprocal relationship to the crystal lattice. This is why the diffraction pattern is often called the "reciprocal lattice." Each diffraction spot represents a group of atomic planes in the crystal and contains information about the distance between atomic planes. The Technai TF20 has built into it the algorithms necessary for considering the effects of the projection lenses, and can measure the d-spacings of a crystal from the spacing of spots in the diffraction pattern.

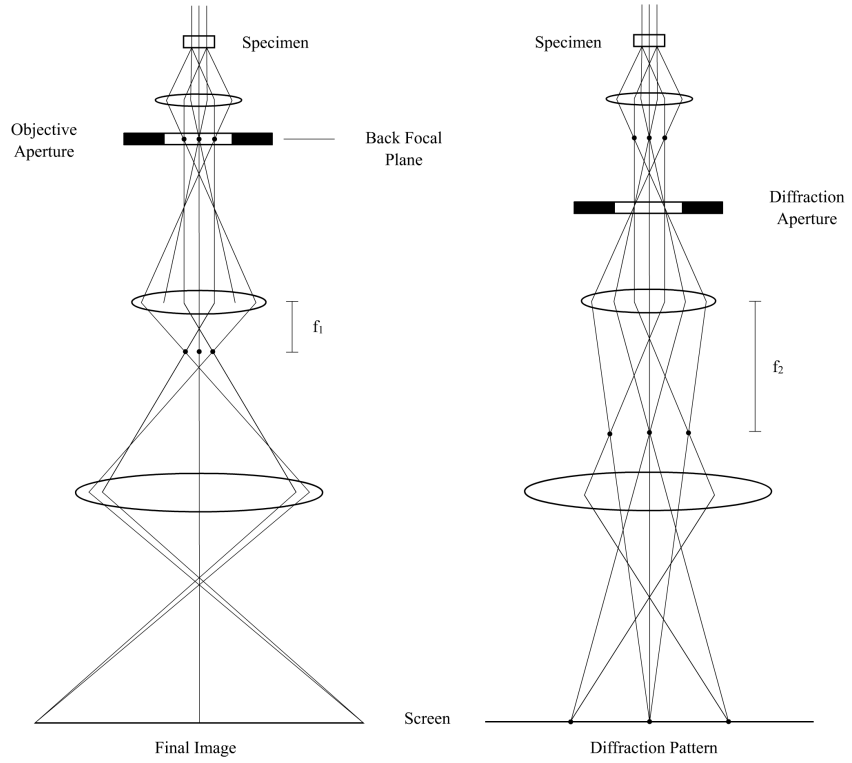

Figure 1.3 TEM Imaging and Diffraction [5]

The objective aperture is much larger than a single nanocrystal, making it necessary to use a second aperture to obtain a diffraction pattern from the crystal without contaminating the pattern with information from its neighbors. For this reason, the diffraction aperture can be inserted to block diffracted rays except those coming from

a limited area around the direct beam. This process is called selected area diffraction (SAD), and is very useful to isolate the diffraction pattern from a small group of crystals, or in some cases, a single large crystal.

SAD is prone to error though. The diffraction aperture must be inserted directly into the image plane, otherwise stray beams still make it to the imagining system and skew the data. Similar problems occur if the specimen of interest is not directly in the eucentric plane - the image occurs at a point before or after the diffraction aperture (see Figure 1.3). Also, selecting an area small enough to isolate one nanocrystal is moderately difficult using the aperture. And as if this wasn't enough, SAD is also particularly sensitive to lens aberrations and astigmatism. Thus, while being none the less useful, for obtaining d-spacing information from a single nanocrystal, SAD leaves something to be desired.

1.2.3 Image Selected Transform Diffraction

Fortunately, there is a way of doing SAD that doesn't rely on the diffraction aperture, and in turn can easily isolate the diffraction patterns from single crystals. Crystals are frequently found in the state of being "in zone," meaning that an axis of the crystal lines up with the axis of the microscope. In this state, the crystal lattice appears as a two dimensional grating to the impinging electrons, which causes electron interference. When viewing a single crystal that is in zone in imaging mode, a series of lattice fringes appear as dark and light bands. These fringe patterns can be described by the two-dimensional Fresnel-Kirchhoff diffraction formula:

$$E(x, y, z = d) = -\frac{i}{\lambda} \int \int_{aperture} E(x', y', z = 0) \frac{e^{ikR}}{R} \left[\frac{(1 + \cos(\mathbf{r}, \hat{z}))}{2} \right] dx' dy' \qquad (1.8)$$

The image screen is far enough away from the crystal that it lies in the far-field,

and thereby the Fraunhofer approximation can be applied,

$$E(x,y,d) = -\frac{ie^{ikd}e^{i\frac{k}{2d}(x^2+y^2)}}{\lambda d}\int\int_{aperture} E(x',y',0)e^{-i\frac{k}{d}(xx'+yy')}dx'dy' \tag{1.9}$$

Because the crystal appears as a two dimensional grating when it is "in zone," the diffraction integral is a two dimensional Fourier transform of the crystal lattice at the specimen plane. Therefore, by performing an inverse Fourier transform on the image of a crystal with a fringe pattern, we can produce a diffraction pattern that is limited to the contents of the image. Thus we remove the need for a selection aperture, and instead select information using the area of the image that illuminates the CCD camera. Through this process it becomes not only possible but easy to isolate the diffraction pattern from a single crystal only a few nanometers wide.

Additionally, this technique is less prone to error. Instead of moving apertures and switching viewing modes, one only needs to capture a quality image on the viewing screen and take its Fourier transform. While overlapping crystals can produce 'false' fringe patterns, these can be avoided by a discerning eye in the selection process.

With a good diffraction pattern, known crystals can be identified by comparison to tabulated values in the Powder Diffraction File (PDF). This way, rutile, anatase, and brookite forms of TiO_2 can be identified, as well as Tellurium metal and its oxides.

1.2.4 XEDS

The TF20 is also capable of X-ray Energy Dispersive Spectroscopy (XEDS). This technique is useful because it can do elemental analysis on the sample and show relative amounts of materials present. XEDS focuses all of the electrons in the beam through a waist about 5 nanometers across which is then called a probe. With so many electrons coming through such a small area, the probe is great for knocking orbital electrons out of atoms in a specific place in the sample. As higher energy

orbital electrons then fall into the holes made, they release an X-ray. The TF20 detects this X-ray and its energy, which information is then compared against known emission spectra until the element that produced the X-ray is identified. Using this method, we can detect and locate materials of interest in our samples.

Chapter 2

Experimental Setup

2.1 Preparing the Samples

Samples are synthesized by a hydrothermal technique. First a solution of $TiCl_4$ and water is made, Tellurium precursor (Te + $NaBH_4$) is added, and the solution is annealed at a fixed temperature between 200°C and 800°C. The result is a powder of tellurium modified TiO_2 nanocrystals. Preparing samples for inspection with the Technai TF20 electron microscope is moderately simple. Because the sample material is a powder of nanocrystals, they can be loaded onto a micro-grid copper sample holder by moving the copper mesh through the powder. This causes enough nanocrystals to get stuck in the mesh that they can be loaded into the microscope and viewed. For samples composed of larger granules, they may have to be crushed using a flat piece of metal. A clean metal surface and the clean back end of some lab tweezers were used to crush these samples. It is important that hydro-carbons are not introduced to the sample as they are attracted to the electron beam and can form carbon pillars on the sample, so the grinding surfaces were thoroughly cleaned before each use.

Using TEM, several particles from each sample were closely inspected for fringe

patterns and crystal size information. Diffraction information was taken using the image capture technique, and elemental information was taken using XEDS. Using XEDS requires going into STEM (Scanning TEM), where the probe is made very small and scanned over the sample. Thus we discovered the presence and location of Te in the samples.

Chapter 3

Results

3.1 Macro Characteristics

The following table describes the color and appearance of the samples made:

Amount of TE present

Baking Temperature	*5% Te*	*10% Te*	*15% Te*
200 C	White *0*	White/Blue *0*	Dark Blue *0*
300 C	Off white *0*	Light Tan *0*	Dark Blue *0*
400 C	Lt Orange *0*	Lt Yellow *0*	Blue/Orange *0*
500 C	Lt Orange *1*	Lt Orange *3*	Yellow *0*
600 C	Orange *2*	Orange *3*	Lt Orange *0*
700 C	Brown *0*	Brown *0*	Orange *0*
800 C	Red/Brown *0*	Red/Brown *0*	Orange *0*

0 = no photodarkening 3 = strong photodarkening

Table 3.1 Macroscopic appearance of samples

Pure TiO_2 is white (the reason it has been used as a base for paint for hundreds

of years). Samples baked at cooler temperatures and higher concentrations of Te produced a dark blue color, almost black. Samples baked at lower temperatures and with less Te were almost white. Higher temperatures produced red to brown powders in samples with more Te, and orange powders in samples with less Te.

3.2 Phase Change of TiO_2

A distinct shift in phase of TiO_2 from the anatase and brookite forms to the rutile form occurs at about 700°C. For all samples annealed at temperatures cooler than 700°C, anatase and brookite are the predominant forms of TiO_2. These two forms produce very similar diffraction patterns when encountered en masse: brookite has it's brightest spot for the 120 plane with a d-spacing of 3.51 Å, while anatase has its brightest spot for the 101 plane with a d-spacing of 3.52 Å. Because of the typical size and abundance of these crystals, it's quite difficult to isolate a single crystal and get a clean diffraction pattern. Instead the pattern usually appears as a series of rings, representing the "signature d-spacings" for those crystals:

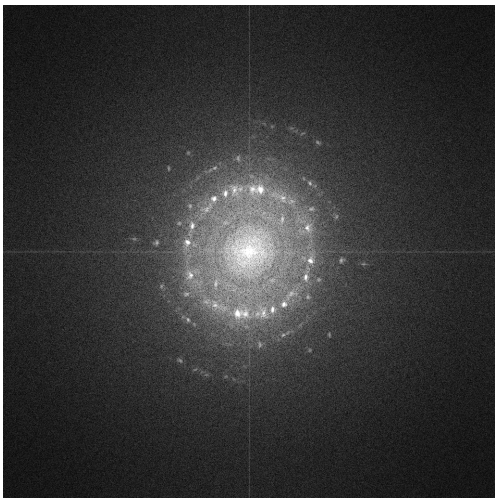

Figure 3.1 The combined diffraction patterns of many similar crystals produces concentric rings.

However, when anatase and brookite can be isolated, it quickly becomes apparent that their underlying structure is quite different. Namely, anatase is a tetragonal structure while brookite is orthorhombic.

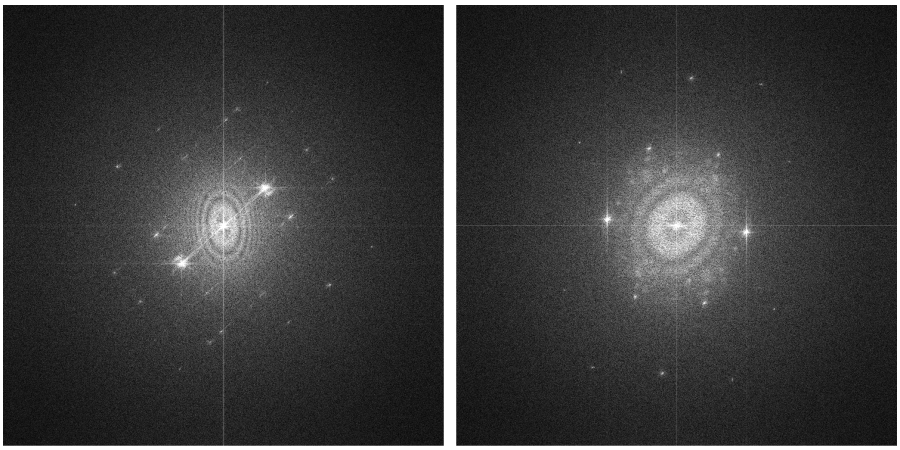

Figure 3.2 Anatase (tetragonal) and brookite (orthorhombic) diffraction patterns showing their different structures.

By comparison with the Powder Diffraction File (see Appendix A), the anatase and brookite forms can be grouped together and identified by their signature d-spacings. The Rutile form, which is tetragonal like anatase, has its brightest spot at 3.25 Å, and subsequent dimmer spots that differ noticeably from those of brookite and anatase. Thus the rutile is easily recognized, and can be identified by comparison with the PDF.

While brookite and anatase are predominant below 700°C, rutile is strongly predominant above 700°C. We concluded that rutile with it's tighter spacings is a more stable form of TiO_2 at higher temperatures.

3.3 Change in TiO_2 Crystal Size

Accompanying the phase change to rutile at 700°C is a dramatic change in size of TiO_2 crystals. Anatase and brookite crystals that form at cooler temperatures are typically 5 to 10 nm in diameter, while the smallest rutile crystals are around 30 to 50 nm across. This leads to somewhat different appearances of the nanoparticles themselves, as well as helps to reveal Te compounds in the higher temperature samples (Figure 3.4).

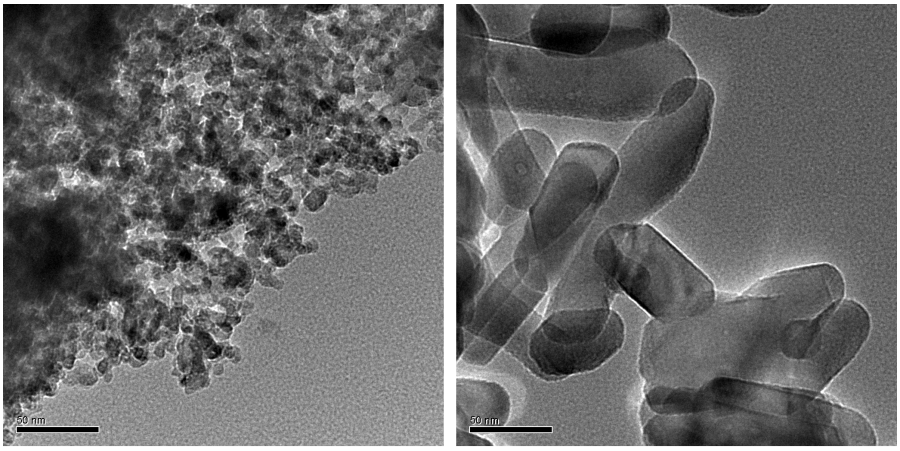

Figure 3.3 Anatase and brookite nanocrystals are on average 5 - 10 nm while rutile ones are around 50nm.

3.4 Finding the Tellurium

XEDS consistently showed the Te is present in roughly the same proportion everywhere in each sample. In high temperature annealed samples where rutile TiO_2 is the predominant form, 10-15 nm diameter particles can still be seen attached to the surfaces of larger crystals. XEDS and diffraction show that these smaller particles are primarily composed of TeO_2. It's possible that these TeO_2 particles are dispersed

throughout every sample and are only revealed when the TiO_2 undergoes the phase change to its rutile form (TeO_2 isn't recorded in the PDF as having multiple phases, therefore it's assumed that it doesn't undergo a phase change similar to that of TiO_2 in this range of temperatures). In low temperature annealed samples, the TeO_2 diffraction pattern is hidden by the strong TiO_2 patterns due to the prevalence of TiO_2. Also, the similarity in size makes TeO_2 nanocrystals visually indistinguishable from TiO_2 nanocrystals. In these high temperature annealed samples though, it can be isolated and identified.

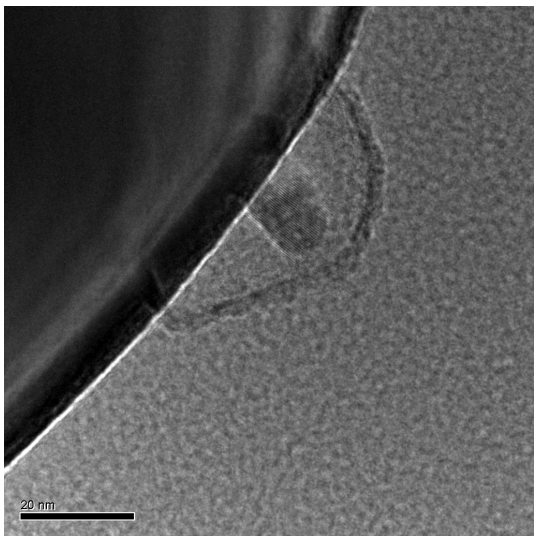

Figure 3.4 A TeO_2 nanocrystal hanging to the surface of a larger rutile TiO_2 crystal

TeO_2 nanocrystals such as the one shown in Figure 3.5 are scattered throughout the nanoparticle, adhering to the surfaces of larger rutile TiO_2 crystals. These particles are very sensitive to the electron beam, however, and disappear if observed for too long. One possible explanation for this is that the smaller particles are only loosely attached to the larger crystals, and the energy delivered by the electron beam, especially when the beam is sharply focused, is enough to knock them loose (Figure 3.5).

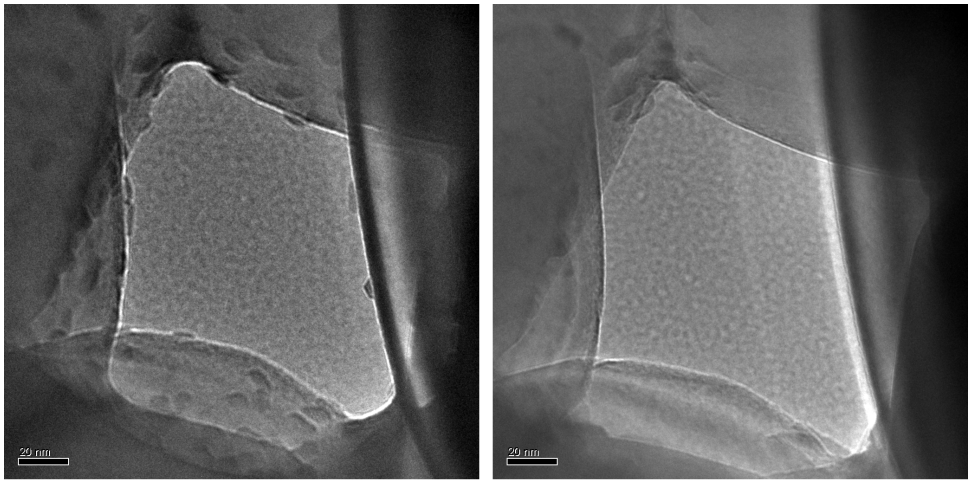

Figure 3.5 TeO_2 nanocrystals spotting the surface of a rutile TiO_2 crystal which burn away under the beam

It's possible that that these small TeO_2 crystals have to do with the photodarkening observed. In the samples where photodarkening did occur, individual TiO_2 crystals did not show Te doping. However, the photodarkening samples were some of those in which anatase and brookite were formed at the upper edge of their temperature range. Also, it was observed that after photodarkening had occurred, these anatase and brookite samples were similar in color to the 700°C and 800°C rutile samples. It's possible that some sort of surface doping, or surface interaction between the TiO_2 and Te or TeO_2 was made possible by the high energy present when these hotter anatase and brookite samples were annealed, and that this surface interaction causes the photodarkening. The high temperature annealed samples where rutile TiO_2 crystals are covered with smaller TeO_2 crystals, may be the permanent version of photodarkened crystals. The permanent color change for the high temperature samples certainly suggests so. Unfortunately, in the photodarkening samples, the similar size of TiO_2 crystals and TeO_2 crystals makes any sort of surface interaction or adhering nearly impossible to observe. The ideal would be to find an anatase or

brookite TiO_2 crystal that had fused at one side with a crystal of TeO_2, or maybe even a clump of fused crystals of both species. Unfortunately, none such structures were found.

While TeO_2 appears in high temperature annealed samples, it should be noted that the Te in cooler samples may not be in a TeO_2 compound, but may simply exist as Te metal, or as a combination of both forms. Unfortunately, the data gathered at present can't tell us if this is the case. Other oxides of Te were not found.

In addition to TeO_2, Te metal was also found in the 700°C - 15% sample, forming relatively large crystals which didn't appear in any other observed samples.

3.5 Conclusions

TEM and XEDS revealed Te as both Te metal and TeO_2 in our samples. We also saw the distinct shift of TiO_2 from anatase and brookite forms to rutile at about 700°C. Because the only samples that displayed photodarkening were those synthesized just below this transition temperature, we think that surface interactions between TiO_2 and Te or TeO_2, made possible by higher annealing temperatures, may play a role in the photodarkening.

Bibliography

[1] P. R. F.Barnes, et. al. "TiO_2 photoelectrodes for water splitting: Carbon doping by flame pyrolysis?," Dev.Chem.Eng.Mineral Proccess **14(1/2),** 51–70 (2006).

[2] S. U. M.Khan, M. Al-Shahry, W. B.Ingler.Jr "Efficient Photochemical Water Splitting by a Chemically Modified n-TiO_2," Science. **297,** 2243–2245 (2002).

[3] K. Hashimoto, H. Irie, A. Fujishima "TiO_2 Photocatalysis: A Historical Overview and Future Prospects," Jap. Journ. App. Phys. **44,** 8269–8285 (2005).

[4] A. J.Nozik, R. Memming, "Physical chemistry of Semiconductor - Liquid interfaces," Journ. Phys. Chem. **100,** 3061–3078 (1996).

[5] P.E. Champness, *Electron Diffraction in the Transmission Electron Microscope*, (BIOS Scientific Publisher Limited, Oxford, 2001), ch. 1 - 2.

[6] J. Peatross, M. Ware, *Physics of Light and Optics*, (Brigham Young University, Utah, 2006), ch. 10.

[7] Joint Committee on Powder Diffraction Standards, *Mineral Powder Diffraction File Data Book*, (International Centre for Diffraction Data, Pennsylvania, 1980), ppg 30, 133, 734, 837, 961, 962.

[8] W. Borchardt-Ott *Crystallography*, (Springer-Verlag Berlin Heidelberg, Germany, 1993), ch. 1 - 2

[9] S. Philips, I. James, B. Hess, "Visible Light Absorbtion and Photo-darkening in Te-modified TiO_2 Nanocrystals," Brigham Young University, 2007

Appendix A

Appendix A:Sample Data from the Powder Diffraction File

4-554

d	3.23	2.35	2.23	3.86
I/I_1	100	37	31	20

Te

Tellurium

(Tellurium)

Rad. $CuK\alpha_1$ λ 1.54050 Filter Ni Dia.
Cut off I/I_1 Diffractometer I/I cor.
Ref. Swanson and Tatge, NBS Circular 539, Vol. 1, 26 (1953)

Sys. Hexagonal S.G. *
a_0 4.4572 b_0 c_0 5.9290 A C 1.331
α β γ Z 3 Dx 6.2259
Ref. Ibid.

$\epsilon\alpha$ $n\omega\beta$ $\epsilon\gamma$ Sign
2V D mp Color Gray
Ref. Ibid.

*$P3_121$ (152) or $P3_221$ (154) [Bradley, Phil. Mag., 48 477-96 (1924)].
Sample obtained from Johnson, Matthey and Company.
Ground and annealed in vacuum furnance at 400°C for 15 minutes. Spectrographic analysis shows Si, Fe, Mg, and Al present at 0.001% or less.
At 26°-27°C.
Merck Index, 8th Ed., p. 1017.
See following card

d A	I/I_1	hkl	d A	I/I_1	hkl
3.86	20	100	1.1740	8	204,213
3.230	100	101	1.1334	3	105
2.351	37	102	1.0951	2	221
2.228	31	110	1.0784	<1	303
2.087	11	111	1.0705	<1	310
1.980	8	003	1.0535	3	311
1.930	4	200	1.0432	2	115
1.835	20	201	1.0399	3	222
1.781	7	112	1.0104	2	214
1.758	2	103	1.0071	3	205,312
1.616	12	202	0.9889	<1	006
1.479	13	113	.9714	2	304
1.459	8	210	.9650	1	223
1.417	8	211	.9413	1	313
1.383	7	104,203	.9201	2	215
1.309	6	212	.9032	2	116
1.287	1	300	.8909	1	224
1.257	4	301	.8858	1	320
1.234	1	114	.8760	1	206
1.1802	3	302	.8719	1	321

4-554A

d	3.23	2.35	2.23	3.86
I/I_1	100	37	31	20

Te

Tellurium

(Tellurium)

Rad. λ Filter Dia.
Cut off I/I_1 I/I cor.
Ref.

Sys. S.G.
a_0 b_0 c_0 A C
α β γ Z Dx
Ref.

$\epsilon\alpha$ $n\omega\beta$ $\epsilon\gamma$ Sign
2V D mp Color
Ref.

See preceding card

d A	I/I_1	hkl	d A	I/I_1	hkl
.8675	4	305,314+			
.8485	<1	322			
.8339	2	411			
.8270	1	107			
.8180	2	216			
.8119	1	225			
.8102	2	412			
.8082	3	404,323			
.7945	2	315			
.7917	1	117			

9-433

d	3.28	3.72	3.01	6.01	TeO_2
I/I_1	100	95	50	5	TELLURIUM OXIDE — TELLURITE

Rad. $CuK\alpha_1$ λ 1.5405 Filter Ni Dia.
Cut off I/I_1 DIFFRACTOMETER
Ref. NAT. BUR. STANDARDS CIRC. 539 9 57-58 (1960)

Sys. ORTHORHOMBIC S.G. D_{2H}^{15} - PBCA (61)
a_o 5.607 b_o 12.034 c_o 5.463 A 0.4659 C 0.4540
α β γ Z 8 Dx 5.75
Ref. IBID.

ε α nωβ ε γ Sign
2V D mp Color COLORLESS
Ref.

SAMPLE (U.S.N.M. # R 8861) ORIGINALLY OBTAINED FROM CANANEA, SONORA, MEXICO. SPECTROGRAPHIC ANALYSIS FROM U.S. GEOLOGICAL SURVEY SHOWED FOLLOWING IMPURITIES: 0.5% Si, 0.3% Cu; 0.2% EACH OF Al, Ba; 0.1% EACH OF Ca, Mg; 0.08% Fe; 0.05% EACH OF Bi, Sn; 0.02% EACH OF Pb, Mn, Sr AND 0.004% Ag. PATTERN MADE AT 25°C. ISOSTRUCTURAL WITH PAKOKSITE (TiO_2). MERCK INDEX, 8TH ED., P. 1017.

d Å	I/I_1	hkl	d Å	I/I_1	hkl
6.01	6	020	1.666	10	123
4.05	12	021	1.6168	8	062,331
3.723	95	111	1.5903	8	133
3.280	100	121	1.5734	4	171
3.008	50	040	1.5176	12	252,213
2.800	25	131,200	1.5021	4	080,143
2.730	45	002,210	1.4662	10	270
2.636	6	041	1.4246	6	351
2.453	10	102	1.4093	8	173
2.298	25	221,230	1.4026	8	181
2.050	20	240,151	1.3267	10	361
2.023	20	042	1.3184	8	082
1.930	25	212	1.2946	12	313,124
1.883	4	061	1.2885	6	253,281
1.826	10	250	1.2708	8	440
1.785	10	161	1.2650	4	191
1.759	20	232	1.2489	8	402
1.750	18	311	1.2434	6	044
1.714	10	113	1.1504	8	1.10.1
1.696	18	321			

11-693

d	2.99	3.40	1.87	4.07	TeO_2
I/I_1	100	85	55	14	TELLURIUM OXIDE — PARATELLURITE

Rad. $CuK\alpha_1$ λ 1.5405 Filter Ni Dia.
Cut off I/I_1 DIFFRACTOMETER
Ref. NAT. BUR. STANDARDS CIRC. 539 10 55 (1960)

Sys. TETRAGONAL S.G. $P4_{1,3}2_12$ (92,96)
a_o 4.810 b_o c_o 7.613 A C 1.583
α β γ Z 4 Dx 6.017
Ref. IBID.

ε α nωβ ε γ Sign
2V D mp Color GREYISH TO COLORLESS
Ref. IBID.

SAMPLE FROM CANANEA, SONORA, MEXICO (USNM R8861). SPEC. ANAL. SHOWED 0.06% Fe; 0.05% Ca; 0.04% Sn, Mg; 0.02% Mn; 0.01% Zr, Ba; AND 0.004% Pb. PATTERN WAS MADE AT 25°C. THE SAMPLE WAS FOUND AS FINE CRYSTALS CO-EXISTING WITH THE ORTHORHOMBIC POLYMORPH (TELLURITE) ON A MATRIX OF NATIVE TELLURIUM. MERCK INDEX, 8TH ED., P. 1017.

d Å	I/I_1	hkl	d Å	I/I_1	hkl
4.068	14	101	1.4129	4	223,312
3.404	85	110	1.3554	<2	303
3.107	14	111	1.3142	4	321
2.988	100	102	1.3048	4	313
2.536	2	112	1.2682	6	224
2.407	20	200	1.2590	8	322
2.296	4	201	1.2431	4	215
2.151	8	210	1.2269	6	106,304
2.071	6	211	1.2026	4	400
2.033	2	113,202	1.1882	8	116,314
1.904	12	004	1.1812	6	323
1.873	55	212	1.1530	4	411
1.746	4	203	1.1339	<2	225
1.701	14	220	1.1214	2	331
1.661	20	114,221	1.1159	4	412
1.641	6	213	1.0929	4	216,324
1.569	4	301	1.0867	2	403,332
1.5212	10	310	1.0760	<2	315,240
1.4925	14	204	1.0646	<1	421
1.4777	10	302	PLUS 2 LINES TO 1.017		

21-1272

d	3.52	1.89	2.38	3.52
I/I_1	100	35	20	100

TiO_2

Titanium Oxide (Anatase)

Rad. $CuK\alpha_1$ λ 1.54056 Filter Mono. Dia.
Cut off I/I_1 Diffractometer $I/I_{cor.}$ =4.3
Ref. National Bureau of Standards, Mono. 25, Sec. 7, 82 (1969)

Sys. Tetragonal S.G. $I4_1/amd$ (141)
a_0 3.7852 b_0 c_0 9.5139 A C 2.5134
α β γ Z 4 Dx 3.893
Ref. Ibid.

$\epsilon\alpha$ $n\omega\beta$ $\epsilon\gamma$ Sign
2V D mp Color Colorless
Ref. Ibid.

Pattern at 25°C. Internal standard: W.
Sample obtained from National Lead Co., South Amboy, New Jersey, USA.
Anatase and another polymorph brookite (orthorhombic) are converted to rutile (tetragonal) by heating above 700°C.
Merck Index, 8th Ed., p. 1054.

d A	I/I_1	hkl	d A	I/I_1	hkl
3.52	100	101	1.0436	4	321
2.431	10	103	1.0182	2	109
2.378	20	004	1.0070	2	208
2.332	10	112	0.9967	2	323
1.892	35	200	.9555	4	316
1.6999	20	105	.9464	4	400
1.6665	20	211	.9246	<2	307
1.4930	4	213	.9192	2	325
1.4808	14	204	.9138	2	411
1.3641	6	116	.8966	4	219,1110
1.3378	6	220	.8890	2	228
1.2795	<2	107	.8819	<2	413
1.2649	10	215	.8793	2	404
1.2509	4	301	.8464	2	420
1.1894	<2	008	.8308	<2	327
1.1725	2	303	.8268	4	415
1.1664	6	224	.8102	2	309
1.1608	4	312	.7974	4	424
1.0600	2	217	.7928	2	0012
1.0517	4	305			

29-1360

29-1361

d	3.51	2.90	3.47	3.51
I/I_1	100	90	80	100

TiO2

Titanium Oxide Brookite

Rad. $CuK\alpha_1$ λ 1.5405 Filter Ni Dia.
Cut off I/I_1 Diffractometer I/I cor.
Ref. Nat. Bur. Stand. (U.S.) Monogr. 25, Sec. 3 (1964)

Sys. Orthorhombic S.G. Pcab (61)
a_0 5.4558 b_0 9.1819 c_0 5.1429 A 0.59419 C 0.56011
α β γ Z 8 Dx 4.120
V 257.63Å^3
Ref. Ibid.

$\epsilon\alpha$ 2.5831 $n\omega\beta$ 2.5843 $\epsilon\gamma$ 2.7004 (Na) Sign +
2V ~28°* D 4.14±.06 mp Color Black
Ref. Dana's System of Mineralogy, 7th Ed., 1 588 (1944)

Specimen from Magnet Cove, Arkansas, USA (USNM 97661).
*2E becomes 0 at 555.5 (25°C).
Spectrographic analysis: 0.1-1.0% Si; 0.01-0.1% each of Al, Fe, and V; 0.001-0.01% Mg. Niobian brookite from Mozambique [Chem. anal.(%): TiO_2 80.7; Nb_2O_5 14.1; FeO 5.53]; Carvalho et al., Rev. Cien. Geol. Ser. A, 7 61 (1974) gives an identical pattern. Pattern was made at 25°C. To replace 16-617.

d A	I/I_1	hkl	d A	I/I_1	hkl
3.51	100	120	1.649	5	151
3.47	80	111	1.610	13	113
2.900	90	121	1.597	2	232
2.729	4	200	1.541	7	123
2.476	25	012	1.494	10	052
2.409	18	201	1.473	4	160
2.370	6	131	1.466	9	312
2.344	4	220	1.461	12	251
2.332	4	211	1.452	12	203
2.296	5	040	1.442	6	152
2.254	8	112	1.434	10	213
2.244	18	022	1.417	9	161
2.133	16	221	1.364	5	400
1.969	16	032	1.336	8	332
1.893	30	231	1.319	3	401
1.851	18	132	1.312	2	233
1.833	3	212	1.285	2	004
1.757	3	240	1.238	10	024,171
1.691	20	320	1.211	2	431
1.662	30	241	10 reflections to 0.982		

21-1276

d	3.25	1.69	2.49	3.25	TiO_2
I/I_1	100	60	50	100	Titanium Oxide (Rutile)

Rad. $CuK\alpha_1$ λ 1.54056 Filter Mono. Dia.
Cut off I/I_1 Diffractometer $I/I_{cor.}$ =3.4
Ref. National Bureau of Standards, Mono. 25, Sec. 7, 83 (1969)

Sys. Tetragonal S.G. $P4_2/mnm$ (136)
a_0 4.5933 b_0 c_0 2.9592 A C 0.6442
α β γ Z 2 Dx 4.250
Ref. Ibid.

εα nωβ εγ Sign
2V D mp Color
Ref.

No impurity over 0.001%
Sample obtained from National Lead Co., South Amboy, New Jersey, USA.
Pattern at 25°C. Internal standard: W. Rutile group.
Two other polymorphs anatase (tetragonal) and brookite (orthorhombic) converted to rutile on heating above 700°C. Merck Index, 8th Ed., p. 1054.

d A	I/I_1	hkl	d A	I/I_1	hkl
3.247	100	110	1.0425	6	411
2.487	50	101	1.0364	6	312
2.297	8	200	1.0271	4	420
2.188	25	111	0.9703	2	421
2.054	10	210	.9644	2	103
1.6874	60	211	.9458	2	113
1.6237	20	220	.9072	4	402
1.4797	10	002	.9009	4	510
1.4528	10	310	.8892	8	212
1.4243	2	221	.8774	8	431
1.3598	20	301	.8738	8	332
1.3465	12	112	.8437	6	422
1.3041	2	311	.8292	8	303
1.2441	4	202	.8196	12	521
1.2006	2	212	.8120	2	440
1.1702	6	321	.7877	2	530
1.1483	4	400			
1.1143	2	410			
1.0936	8	222			
1.0827	4	330			